Combined magnetic-dipole and electric-quadrupole hyperfine interactions in rare-earth orthoferrite ceramics

Todd M. Rearick, Gary L. Catchen, and James M. Adams
Department of Nuclear Engineering and Electronic Materials and Processing Research Laboratory, The Pennsylvania State University, University Park, Pennsylvania 16802
(Received 12 October 1992; revised manuscript received 25 January 1993)

Perturbed-angular-correlation (PAC) spectroscopy was used to measure combined nuclear-magnetic-dipole and nuclear-electric-quadrupole interactions in rare-earth orthoferrite (REO) ceramics, $R\mathrm{FeO}_3$ (R=La,Pr,Nd,...,Lu). The rare-earth orthoferrites are canted antiferromagnets that have orthorhombically distorted perovskite structures. With the $^{111}\mathrm{In}\rightarrow{}^{111}\mathrm{Cd}$ probe, the PAC measurements were made over a temperature range from laboratory temperature through the antiferromagnetic-to-paramagnetic transitions (740–620 K) and at or near 800 K. In the heavier REO's, the $^{111}\mathrm{In}\rightarrow{}^{111}\mathrm{Cd}$ probe substitutes primarily into the rare-earth sites; and in the lighter REO's, it can substitute into both the Fe and the rare-earth sites. At the rare-earth sites, the probe undergoes a high-frequency electric-quadrupole interaction that is shifted in energy by a weak magnetic-dipole interaction. The direction of the associated magnetic hyperfine field is nearly perpendicular to the principal z axis of the electric-field-gradient (EFG) tensor. The magnitude of this field is small, and it may be produced by transferred spin density. In the heavier REO's, the rare-earth-site EFG's are nearly axially symmetric; and, as the rare-earth atomic number decreases, the EFG asymmetry increases. At the Fe sites, the probe undergoes a strong magnetic-dipole interaction that is shifted in energy by a low-frequency electric-quadrupole interaction, which involves very asymmetric EFG's. For PrFeO_3, as an example, the strong magnetic-dipole interactions could be attributed to the presence of a supertransferred hyperfine field in which spin density is transferred via Fe-O-^{111}Cd bonds. The predictions of a quantum-chemistry theory agree within a factor of 2 with the magnitude of this field. The direction of this field makes an angle of approximately 40° with the principal z axis of the EFG. For NdFeO_3, similar results were obtained. The results of these experiments indicate that combined interactions can be measured in highly distorted crystals and that they can be analyzed. Moreover, these results indicate that PAC spectroscopy can provide new information about the magnitudes and directions of supertransferred hyperfine fields, which can be used as benchmarks for theoretical calculations.

I. INTRODUCTION

The rare-earth orthoferrites (REO's) $R\mathrm{FeO}_3$ (R=La, Pr,...,Lu, and Y) undergo several unusual types of magnetic-ordering phase transitions, and all of the REO's have similar orthorhombically distorted perovskite structures, which have low symmetries. For these reasons, and because they have received much experimental and theoretical investigation,[1–15] we identified the REO's as good candidates for a perturbed-angular-correlation (PAC) spectroscopy investigation. The REO's provide an opportunity to test the theory of the combined magnetic dipole, electric-quadrupole interaction as it applies to low-symmetry hyperfine interactions in a group of magnetic compounds, which have properties that change systematically as a function of the rare-earth composition. In particular, the orthorhombic distortions of the REO perovskite structures give rise to large electric-field-gradients (EFG's) at the rare-earth sites, which are nearly axially symmetric in the heavier rare-earth compounds, and to small EFG's at the Fe sites, which are asymmetric in the lighter rare-earth compounds. At laboratory and elevated temperatures, the magnetic hyperfine fields (MHF's) are very small at the rare-earth sites and large at the Fe sites. These structural features suggest that a variety of interesting combined interactions could be measured using the $^{111}\mathrm{In}\rightarrow{}^{111}\mathrm{Cd}$ probe. The extent of this investigation would depend strongly on the site substitution of the probe. Moreover, the resulting PAC measurement may provide complementary information about MHF's in these materials.

Approximately three decades ago, the theory of the combined nuclear-magnetic-dipole and nuclear-electric-quadrupole interaction was developed.[16–19] This theory applies to both Mössbauer-effect (ME) and perturbed-angular-correlation experiments. Generally, in ^{57}Fe ME experiments on magnetically ordered materials, strong magnetic-dipole interactions of the excited ^{57}Fe nuclei with local MHF's have been measured. In these experiments, the interactions of the nuclear-electric-quadrupole moments with local EFG's generally have produced small effects. Alternatively, PAC measurements on magnetically ordered materials, for the most part, have been performed on highly symmetric crystals that generate either small or vanishing EFG's at the probe sites. In particular, Rinneberg and Shirley have used PAC spectroscopy via the ^{111m}Cd probe to measure supertransferred MHF's at impurity-probe sites in cubic metal oxides[20] and at the transition-metal sites in metal-fluoride perovskites.[21] Prior to these studies, Shirley, Rosenblum, and Matthias[22]

and Shirley and Westenbarger[23] have measured and systematized hyperfine fields in various cubic metals. Hohenemser, Rosov, and Kleinhammes have used PAC spectroscopy to measure critical phenomena in a variety of primarily cubic ferromagnetic and antiferromagnetic materials.[24] In most of these cases, magnetic hyperfine interactions have been observed in which electric-quadrupole interactions either vanished or were insignificant. Moreover, the presence of both MHF's and EFG's can complicate the analysis of the associated PAC measurements to the extent that obtaining accurate interaction frequencies becomes problematical. A noteworthy exception is the investigation by Saylor *et al.* of the effects of O stoichiometry in antiferromagnetic La_2CuO_4 for which they used the $^{111}In \rightarrow {}^{111}Cd$ PAC probe.[25] In these measurements, they assigned the probe substitution to the La site.[25] Compared to the strength of the electric-quadrupole interaction, the effects of the MHF at the La site in La_2CuO_4 are relatively weak and are directed approximately perpendicular to the major EFG axis. These features facilitated the analysis of the combined interactions.

The REO's are magnetically ordered perovskites that have structures represented by the space group *Pbnm* (D_{2h}^{16}). The corresponding unit cell has orthorhombic symmetry and it contains four Fe sites and four-rare earth sites that are crystallographically equivalent. Magnetic ordering can make these sites inequivalent and give rise to four distinct Fe sublattices. For practical purposes, a two-sublattice model of the structure provides an accurate representation.[6,12,13] Figure 1 presents a diagram of the structure. The REO's are canted antiferromagnets that, as a result of the canting, show weak ferromagnetism. They have high-transition temperatures that monotonically decrease as the rare-earth atomic number increases,[15] $T_N = 743$ K for $LaFeO_3$ and $T_N = 625$ K for $LuFeO_3$.[6]

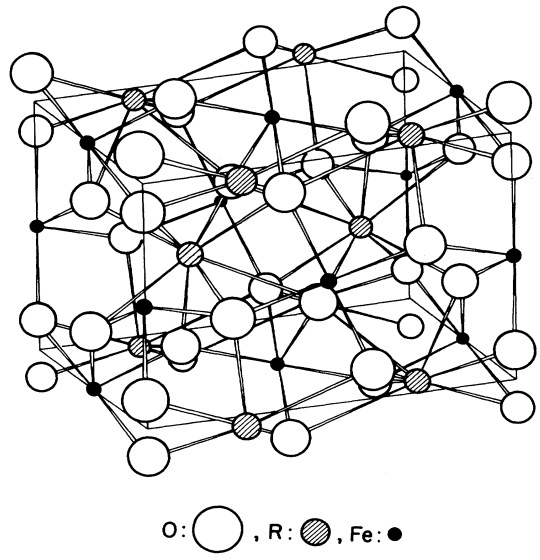

FIG. 1. Structural diagram of the rare-earth orthoferrite unit cell, which is viewed from the *b* axis.

At the higher temperatures, the antiferromagnetic axis lies along the *a* axis of the crystal. Because the associated Fe magnetic moments are canted, the crystal has a net, small macroscopic magnetization along the *c* axis. The canting angles range from 9 to 11 mrad.[5] For REO's that have paramagnetic rare-earth ions, the rare-earth exchange interactions are very weak, and the magnetic ordering of the rare-earth ions occurs only at very low temperatures of several K. At intermediate temperatures, interactions between Fe^{3+} and rare-earth ions that have nonpaired *f* electrons become important, and spin-reorientation transitions can occur.[4] During these transitions, as the temperature decreases, the direction of the antiferromagnetic axis changes from being aligned along the *a* axis to being aligned along the *c* axis and the net magnetization then points along the *a* axis.[4] Most of these spin-reorientation transitions occur at temperatures that are well below laboratory temperature. The exception is $SmFeO_2$, which undergoes the transition at ≈ 480 K.[4]

As a group, the REO's exhibit magnetic properties that depend strongly on the effects of directional chemical bonding. At higher temperatures, the magnetic ordering involves primarily the Fe^{3+} ions that undergo superexchange interactions via Fe^{3+}—O^{2}—Fe^{3+} bonds. (The bond angle in the *c* direction differs from those in the *a* and *b* directions.) The associated average cosine squared of these bond angles is largest for $LaFeO_3$ (157°) and smallest for $LuFeO_3$ (142°). The magnetic-hyperfine fields at the Fe nuclei, which were determined from ME measurements,[5] increase linearly with the average cosine squared of the bond angles.[15] Spin-density transfer via the O ligands produces the supertransferred contribution to the hyperfine fields at the Fe nuclei, and this contribution also has a strong cosine-squared dependence on the Fe—O—Fe bond angle. Whereas, the contribution to the Fe-site hyperfine field from the Fe *d* electrons, which superexchange polarizes, does not have this strong angular dependence.[15] However, the magnitude of the Fe *d*-electron exchange constant does depend strongly on the cosine squared of the Fe—O—Fe bond angle. The larger overlap of electron orbitals, which results from larger Fe—O—Fe bond angles, gives rise to correspondingly larger superexchange interactions that result in larger T_N values. For this reason, T_N, which is proportional to the exchange constant, changes linearly with the average cosine-squared of this angle.

As far as we know, Eibschütz, Shtrikman, and Treves[5] performed the only systematic, extensive measurements of hyperfine interactions in the REO's, for which they used ^{57}Fe (resonant absorption) ME spectroscopy. This investigation determined the dependence of the Fe-site MHF on temperature as well as on rare-earth composition. The ME experiment offers the advantage that it can be used to measure the Fe-site MHF very accurately. Also, for this purpose, the effects of electric-quadrupole interactions do not complicate the analysis in any significant way. Typically, at laboratory temperature, the ME spectra shows six sharp lines that represent the magnetic hyperfine interaction, which include the effects of very small quadrupole coupling constants, <0.05

mm sec^{-1}.[5] However, in the ME measurements, the derived MHF includes contributions from the superexchange that involve Fe *d* electrons and contributions from the supertransferred hyperfine field that involve the transfer of spin through O-ligand *p* orbitals to Fe *s* and *d* orbitals.[15] This situation is neither an advantage nor a disadvantage, it just defines the scope of the ME experiment.

The PAC experiment, on the other hand, exhibits quite a different range of sensitivities. In particular, to measure MHF's and EFG's, the PAC technique uses impurity probes such as $^{111}\text{In}\rightarrow{}^{111}\text{Cd}$, ^{111m}Cd, and $^{181}\text{Hf}\rightarrow{}^{181}\text{Ta}$ that are substituted into specific sites in the crystal of interest in either small or trace amounts. This feature means that PAC measurements could be made on related perovskite compounds such as $R\text{CoO}_3$ and $R\text{MnO}_3$. Although, in principle, ^{57}Fe ME spectroscopy could be performed on these non-iron-containing compounds by doping them with ^{57}Co source atoms, the level of experimental difficulty and expense would be much greater. Furthermore, either in the REO's or in related perovskites, ME measurements are limited to investigating the transition-metal site. Whereas, depending on the crystal chemistry of the PAC (parent nucleus) probe, ^{111}In, for example, it may be possible to use PAC to measure hyperfine interactions either at both metal sites or at one of the metal sites in the REO's, or at none of them. Moreover, at either of the metal sites in the REO's, the $^{111}\text{In}\rightarrow{}^{111}\text{Cd}$ probe, for example, could measure the supertransferred hyperfine field (STHF) in the absence of the effects of *d*-electron superexchange, because the (daughter nucleus) probe, ^{111}Cd in this case, has a closed *d*-electron shell. If the probe were to substitute into both sites in measurable amounts, then the measured STHF's at the two sites could be compared. This comparison could provide a means to test theoretical calculations of transferred spin densities. However, in this context, we offer a caveat. The actual STHF that would be measured is the STHF at an impurity probe nucleus. This field could differ somewhat from the STHF produced at either a Fe or a rare-earth nucleus because the ^{111}Cd probe atom differs in electronic structure from the native-atom structures.

To investigate these possibilities, we have measured combined interactions in ceramic samples of the REO's at laboratory and elevated temperatures using the $^{111}\text{In}\rightarrow{}^{111}\text{Cd}$ PAC probe. We have addressed three major questions: (1) Can well-defined combined magnetic-dipole, electric-quadrupole interactions be measured in the REO's using the $^{111}\text{In}\rightarrow{}^{111}\text{Cd}$ PAC probe and can the probe site be uniquely identified? (2) If so, can unique interaction frequencies be obtained from the primary experimental time distributions and can these interaction frequencies be analyzed using a simple model that we base on the aforementioned theory?[16–19] (3) Can the MHF's, EFG's, and the associated angle between the MHF direction and the principal *z* axis of the EFG be estimated with sufficient precision and confidence so that additional information can be deduced about MHF's in the REOs, which can be used as benchmarks for theoretical calculations?

II. EXPERIMENTAL DETAILS

A. Sample preparation

Ceramic samples of the various REO's were prepared using two methods, coprecipitation and resin intermediate. The coprecipitation method involved dissolving accurately weighted amounts of rare-earth nitrates and $\text{Fe(NO}_3)_3\cdot 9\text{H}_2\text{O}$ in H_2O. The carrier-free $^{111}\text{In}\rightarrow{}^{111}\text{Cd}$ probe was added via a small volume of $^{111}\text{InCl}_3$ in 0.05-M HCl solution, which contained 10 ± 5 μCi of activity. The solution was boiled to reduce the volume and subsequently precipitate the nitrates. The precipitate mixture was pressed into small pellets and sintered in air in a tube furnace. The resin-intermediate method involved dissolving the same precursor compounds in a solution of ethylene glycol and citric acid. An ^{111}In-probe-containing solution was added, and the resulting solution was heated to form a polyester resin in which the metal ions were chelated. The resin was pyrolized using a hot plate, and the residue was subsequently calcined in a box furnace at approximately 1200 K. The resulting powder was pressed into small pellets and sintered. After the pellets were sintered, the PAC measurements were performed. Although the resin-intermediate method offers some well-known advantages such as providing a reliable pathway to homogeneously mix the precursor metal ions and the probe ions, the coprecipitation method is a simpler way to prepare the REOs. Despite the differences in the methods, we observed no salient differences in the sample quality that we could attribute to either method. For samples prepared by either method, the sintering temperatures varied over a range from 1400 to 1800 K, although most of the samples were sintered at temperatures above 1600 K. The variation in sintering temperature arose because we observed changes in the probe-site substitution in some of the REO's. We observed little variation in crystallinity with differences in sintering temperatures. Efforts were made to reduce the potential errors associated with weighing the hygroscopic reagents. We estimate that these errors contributed an error of no more than 1 at.% to the stoichiometry of the prepared samples. To check the phase purity of the radioactive samples, x-ray-diffraction patterns were measured on small amounts of powder taken from each of the samples. For the most part, the samples were composed of a single phase to within several percent. Figure 2 presents two typical diffraction patterns. Additionally, a simple tube furnace was used to maintain the elevated temperatures during the PAC measurements, which was controlled to ± 1 K.

B. PAC measurements

A recent paper[26] and a review[27] present most of the experimental details involved with performing and analyzing conventional PAC experiments. We measured combined interactions that represent two very different experimental situations: namely, that of a weak MHF and a strong EFG and that of a strong MHF and a weak EFG.

Most of the experimental time distributions were col-

lected using a four-CsF-detector PAC apparatus, which has a time resolution of ≈ 1 nsec, full width at half maximum (FWHM), and which collects eight (four 90° and four 180°) coincidences concurrently. Some of the time distributions were collected using a more-recently-acquired four-BaF_2-detector PAC apparatus, which has a time resolution of ≈ 800-psec FWHM and which collects four coincidences concurrently. The experimental perturbation functions $A_{22}G_{22}(t_i)$ were obtained from the measured correlation functions, i.e., time distributions, $W_{jk}(\theta_{jk},t_i)$ that represent the primary experimental data (the subscripts j and k refer to the coincidence between the respective detectors, and i refers to the time interval). Specifically, the ratio method was used to obtain $A_{22}G_{22}(t_i)$, which Eq. (1) in Ref. 26 gives for eight coincidences and which Eq. (8) in Ref. 27 gives for four coincidences.

Because we found no significant precedents in the literature, we present detailed descriptions of the new methods of analysis that we developed as well as the relevant information about the conventional aspects of the analysis.

1. Electric-quadrupole interactions

To analyze the perturbation functions in which no effects of magnetic hyperfine interactions were evident, i.e., those measured at temperatures above T_N, we used a two-site model for nuclear electric-quadrupole interactions in a polycrystalline source:

$$-A_{22}G_{22}(t_i)=A_1\left[S_0(\eta_1)+\sum_{k=1}^{3}S_k(\eta_1)\exp\left[\frac{-1}{2}(\delta_1\omega_k t_i)^2\right]\cos(\omega_k t_i)\right]$$
$$+A_2\left[S_0(\eta_2)+\sum_{k=4}^{6}S_k(\eta_2)\exp\left[\frac{-1}{2}(\delta_2\omega_k t_i)^2\right]\cos(\omega_k t_i)\right]+A_3\ . \quad (1)$$

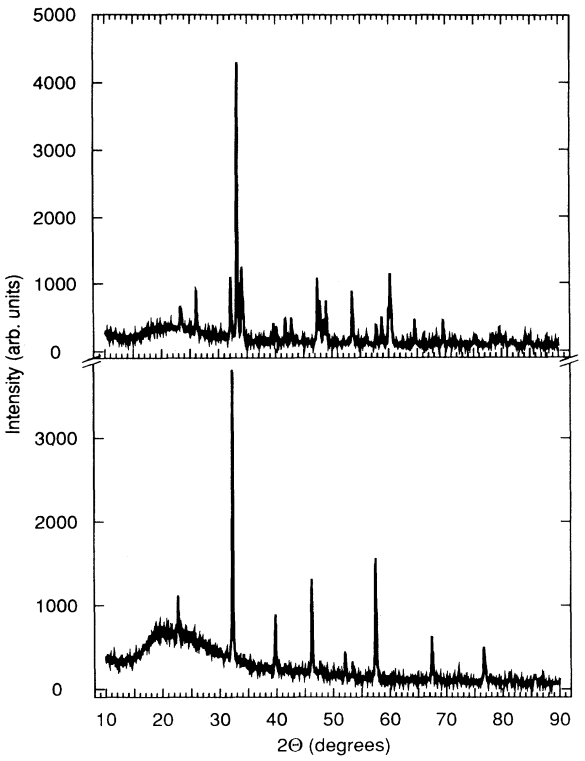

FIG. 2. X-ray powder diffraction patterns for $LaFeO_3$ (lower) and $HoFeO_3$ (upper) ^{111}In-doped ceramic samples. The differences in crystal symmetry are evident. The pattern for $LaFeO_3$ shows relatively few peaks, which indicates near tetragonality; and the pattern for $HoFeO_3$ shows a large number of peaks characteristic of orthorhombic distortion.

Here A_1 and A_2 are the normalization factors, δ_1 and δ_2 are the line-shape parameters, which give the relative widths of Gaussian frequency distributions (of the corresponding sets of $\omega_k s$) that give rise to static line broadening, and A_3 takes into account the effects of γ rays that the sample absorbs and the effects of the probe atoms that are not in well-defined chemical environments, namely, either site one or site two. The frequencies ω_k and the $S_k(\eta)$ coefficients describe a static interaction in a polycrystalline source.[27] Equation (1) was fitted to each of these perturbation functions, and the free parameters for site one $(A_1,\delta_1,\omega_1,\omega_2)$, those for site two $(A_2,\delta_2,\omega_4,\omega_5)$, and A_3 were derived from the fits. In these fits, the constraints $\omega_3=\omega_1+\omega_2$ and $\omega_6=\omega_4+\omega_5$ and $\omega_1\le\omega_2\le 2\omega_1$ and $\omega_4\le\omega_5\le 2\omega_4$ were applied, and the $S_k(\eta)$ coefficients were determined from each set of frequencies. For each site, the ratios ω_2/ω_1 and ω_5/ω_4 were used to determine the corresponding quadrupole frequencies ω_Q and asymmetry parameters η. The nonvanishing EFG components V_{ii} in the principal-axis system where the probe nucleus is at the origin are related to the quadrupole frequency ω_Q and the asymmetry parameter η by $\omega_Q=[eQV_{zz}/4I(2I-1)\hbar]$ and $\eta=(V_{xx}-V_{yy})/V_{zz}$, in which Q is the nuclear quadrupole moment (0.77 b) of the spin $I=\frac{5}{2}$ intermediate nuclear level in the ^{111}Cd probe nucleus. The site-occupancy fractions are given by $f_i=A_i/(A_1+A_2+A_3)$, $i=1$, 2, and 3.

2. Combined interactions

To analyze the perturbation functions that showed the effects of both magnetic dipole and electric-quadrupole

interactions, we used the theory of the combined interaction.[16–19] In this theory, the eigenvalues of the Hamilton matrix depend on $y=\omega_L/\omega_Q(\eta)$ and on the angles β and α. The Larmor frequency, $\omega_L=g\mu_N H/\hbar$, characterizes the magnetic hyperfine interactions, in which H is the MHF at the probe nucleus, μ_N is the nuclear magneton, and g is the corresponding nuclear g factor (-0.306).[20] The angle β gives the direction of the MHF with respect to the z axis of the EFG; and, when $\eta\neq 0$, the angle α gives the orientation of the x-y axis of the EFG in the x-y plane. In general, to analyze perturbation functions produced by combined interactions requires identifying up to primarily nine frequency components (for $I=\frac{5}{2}$) that can contribute to $G_{22}(t)$, when the probe occupies only a single site. These components are produced by m-to-m' transitions in which m-$m'=\pm 1,\pm 2$. Additionally, multiple interactions that can have frequency components in common, which probes substituting into more than one site in the crystal can cause, can complicate the analysis to the point that characterizing the combined interaction becomes problematical. To fit the perturbation functions, we used a model for a combined interaction in a polycrystalline source:

$$-A_{22}G_{22}(t_i)=S_0+\sum_{k=1}^{n} S_k \exp\left[\frac{-1}{2}(\delta\omega_k t_i)^2\right]\cos(\omega_k t_i)\ , \quad (2)$$

in which n is the total number of frequencies. This model uses a single Gaussian line-shape factor. In the fitting process, the S_k coefficients, the line-shape parameter δ, and the frequencies ω_k were treated as free parameters, and no sum constraints were used. We treated the S_k coefficients as free parameters for two reasons, rather than using fixed values that we specified. First, we intended the model to be generally applicable to combined interactions, in which case the S_k coefficients may not be known *a priori*. Second, the perturbation functions for the REO's generally showed the effects of multiple interactions, although the combined interactions of interest produced the dominant effect. To take the secondary interactions into this account, we used as many frequency components as necessary. In the case of weak magnetic hyperfine interactions (MHI's), the primary, combined-interaction data often could be fit using only five frequency components. In the case of strong magnetic hyperfine interactions, up to 14 frequency components were used to fit the data in which 9 frequencies represented the large-amplitude components of the strong MHI and the other frequencies represented other interactions. Thus, as a matter of simplicity and convenience, we treated the S_k coefficients as free parameters. One possible disadvantage of this model is that the line-shape factor, which includes only one parameter δ, multiplies each frequency component. A more general model would include one line-shape factor to multiply the combined-interaction frequency components and at least one other line-shape factor to multiply the other components. Despite this shortcoming, the model provided reasonably good representations of most of the perturbation functions of interest.

The fits of Eq. (2) to the perturbation functions produced a set of frequencies ω_k and experimental S_k coefficients for the primary combined interaction as well as a set of additional frequencies and S_k coefficients. Thus, fits involving n frequencies were performed by varying $2n+2$ free parameters.

(a) Weak magnetic hyperfine interactions. Figure 3 illustrates the dependence of the eigenvalues on η for $y=0.25$ and for several values of the angle β, which are typical for weak MHI's. Some of the interactions that we measured represent a limiting condition; namely, η is small, $\beta\approx 90°$, $y<1$, which corresponds to a weak MHI directed nearly perpendicular to the EFG that perturbs a strong, nearly axially symmetric electric-quadrupole interaction. The small η values cause the α dependence to be very weak. The large-β values cause the $m=\pm\frac{5}{2}$ and $\pm\frac{3}{2}$ states to remain nearly degenerate. When large β values occur with small-y values, for example, $y=0.25$, the primary interaction frequency ω_1 is split into two components, and the secondary frequency ω_2 is essentially not split. Thus, for this limiting condition, we have to determine five separate frequencies of which two are related to the other three. Using the notation in Fig. 3, we note that $\omega_3=\omega_1+\omega_2$ and $\omega_6=\omega_4+\omega_5$, in which $\omega_2=\omega_5$ and in which ω_1 and ω_4 differ by very little, i.e., $|\omega_1-\omega_4|\ll(\omega_1+\omega_4)/2$.

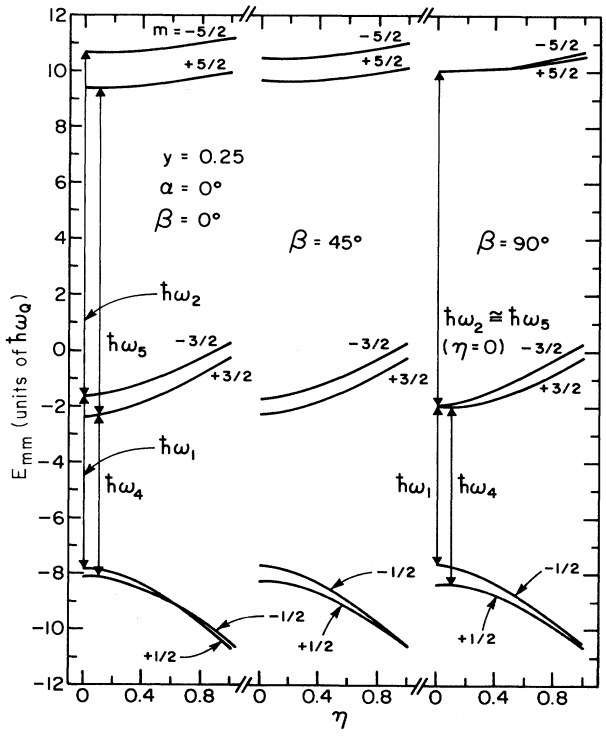

FIG. 3. Energy level diagram for a spin $I=\frac{5}{2}$ nuclear-electric-quadrupole interaction, in which a weak magnetic hyperfine field lifts the twofold degeneracy of the $\pm m$ states; η is the EFG asymmetry, and $y=\omega_L/\omega_Q$. When β is close to 90° and η is small, the frequencies ω_2 and ω_5 are nearly degenerate, and for practical purposes, as long as y remains small, ω_2 and ω_5 cannot be separated experimentally.

Usually the fits provided accurate values of ω_2, which could not be distinguished from ω_5. But either ω_1 or ω_4 or both ω_1 and ω_4 had significantly more uncertainty associated with them. As a result, usually the sum frequencies ω_3 and ω_6 were poorly defined. These uncertainties limited the accuracy with which we were able to determine the primary interaction parameters V_{zz}, η, β, and y.

To determine these parameters that characterize the combined interaction for the aforementioned limiting condition, we calculated two ratios $R_{21}=\omega_2/\omega_1$ and $R_{54}=\omega_5/\omega_4$ using the derived experimental frequencies, and we set a third ratio $R_{25}=(\omega_2/\omega_5)=1$. We used the published combined-interaction matrix elements [H'_{mm} in Eq. (9) of Ref. 19] to calculate the Hamilton matrix for various values of η, α, β, and y, and we found the corresponding eigenvalues and the eigenvectors that diagonalize the Hamilton matrix. Using these eigenvalues for the specific values of η and α, we formed matrices of the theoretical ratios R_{21}, R_{54}, and R_{25}, in which each matrix element corresponds to a specific ratio R_{ij} for a pair of y and β values. To find the values of y and β that best represented the combined interaction, for specific η and α values, we searched the three ratio matrices for the set of theoretical ratios that minimized the squared differences between the theoretical and the experimental ratios, χ^2:

$$\chi^2_{ij}=[(R_{21})_{ij}-(R_{21})_{\text{expt}}]^2+[(R_{54})_{ij}-(R_{54})_{\text{expt}}]^2 + [(R_{25})_{ij}-(R_{25})_{\text{expt}}]^2 , \quad (3)$$

in which the indices i and j refer to a specific pair of y and β values. For this limiting condition, we set $(R_{25})_{\text{expt}}=1$. This method is rather sensitive to the η values as well as to the y and β values. But when η is small, the method is not very sensitive to the angle α. So we treated α as a phenomenological parameter to which we could not ascribe any physical significance.

(b) Strong magnetic hyperfine interactions. For $LaFeO_3$, $PrFeO_3$, $NdFeO_3$, and $SmFeO_3$, the probe-site substitution depends strongly on the sintering temperatures. (For the other, heavier REO's, we did not investigate this phenomena as extensively, and presently, we cannot offer more definitive information about probe-site substitution.) Lower sintering temperatures, e.g., 1400–1500 K, tend to enhance substitution of ^{111}In into the Fe sites, and higher temperatures tend to enhance probe substitutions into the rare-earth sites. (We present the rationale for assigning the site occupancies below.) For a specific sample, we determined the relative site-occupancy fraction by analyzing a PAC measurement made at $\approx$800 K. Since this temperature exceeds T_N for all the REO's, we observed only pure electric-quadrupole interactions in these 800-K measurements. The frequencies corresponding to the interactions at the two metal-ion sites differ markedly in magnitude. Typically, for the Fe-site interaction, ω_1 ranges from 20 to 40 Mrad sec^{-1}, and for the rare-earth-site interactions, ω_1 ranges from 150 to 170 Mrad sec^{-1}. So the site substitutions were easy to identify. However, at temperatures below T_N, the strong MHI's at the Fe sites give rise primarily to nine frequency components. The lower five of these components correspond to transitions in which $m-m'=\pm1$ (of these, the $\frac{1}{2}\leftrightarrow-\frac{1}{2}$ transition is very weak and not resolvable); and upper four correspond to transitions in which $m-m'=\pm2$. Typically, the lower five components have magnitudes that range from 50 to 200 Mrad sec^{-1}. Because generally the frequency components that correspond to rare-earth-site interactions are also present in the perturbation functions, the complete frequency sets that characterize the strong, Fe-site MHI's cannot be unambiguously identified. Usually we were able to identify some but not all of the frequency components. In the measurements on $PrFeO_3$, we observed very little probe substitution into the rare-earth site, and we obtained more complete frequency information than we could from measurements on the other samples. An additional ambiguity arises because some of the frequency components that correspond to a strong MHI may not be experimentally resolvable. Thus, two effects exacerbate the difficulties associated with analyzing the combined-interaction data: (1) true strong MHI frequency components that are nearly degenerate and (2) frequency components that have similar magnitudes to some of the true strong-MHI components, which arise from interactions at other sites.

To analyze the perturbation functions, we fitted them using Eq. (2). Then we attempted to identify the frequency components that the strong MHI appeared to have generated. For this purpose, we used the power-law dependence of the ω_i's on reduced temperature, $t_r=1-(T/T_N)$, in which $\omega_i(t_r)=\omega_i(0)t_t^{\beta}$, to qualitatively separate frequency components that have the appropriate temperature dependence from those that do not. (The exponent β is not to be confused with the angle β mentioned above.) Specifically, the frequency components that the strong MHI would have generated should give a temperature dependence for which $\beta=0.348$,[5] and those components generated by other interactions should give a very weak temperature dependence. At temperatures near T_N, the strong MHI components could not be resolved. At temperatures roughly 100 K or more below T_N, at least several components could be resolved. Generally, we could resolve the four higher-frequency components more reliably than the five lower-frequency components.

After we obtained the sets of frequency components that characterize the strong MHI at each temperature, we proceeded to estimate the parameters η, β, α, and y that characterize the combined interaction. For this purpose, we generated sets of frequencies $\omega_i(\eta,\beta,\alpha,y)$ from the eigenvalues of the Hamilton matrix for arrays of values of η, β, α, and y. To determine the set of these parameters that is the best representation of the measured frequencies, we performed a grid search to find the set of theoretical frequencies that minimized the sum of the squared differences between the theoretical and the experimental frequencies, χ^2:

$$\chi^2=\sum_{i=m}^{n}[\omega_i(\eta,\beta,\alpha,y)-(\omega_i)_{\text{expt}}]^2 , \quad (4)$$

in which m and n specify the frequencies used in the search, e.g., for the upper four frequencies, $m=5$ and $n=9$. Unfortunately, for the frequency sets that we mea-

sured, this method did not generate unique sets of parameters. To obtain a self-consistent set of parameters for each of the REO's, we needed to constrain the search by specifying ω_Q and η. For this purpose, for a given set of experimental frequencies, we approximated the Larmor frequency as $\langle\omega_L\rangle=(\sum_{i=m}^{n}\omega_i)/(n-m)a$, in which $a=1$ when the lower frequencies are averaged and $a=2$ when the upper frequencies are averaged. Using this value of $\langle\omega_L\rangle$ and the specified value of ω_Q, we could fix the value of the parameter $y=\langle\omega_L\rangle/\omega_Q$. Since we could not obtain values of ω_Q and η for the below-T_N measurements directly, we used the values of ω_Q and η measured at 800 K. Thus, using this constrained search procedure, in which the values of η and y remained fixed, we were able to find self-consistent sets of β values for a specified value of α. In this procedure, the tacit assumption is that ω_Q and η have a weak temperature dependence. The self-consistency of the resulting β values supports this assumption.

III. RESULTS

The experimental results consist of four sets of measurements: (1) combined interactions at the rare-earth sites measured at laboratory temperature on most of the REO's, in which the MHF is relatively weak, i.e., $y \ll 1$, (2) temperature dependence of these combined interactions measured between laboratory temperature and T_N on several REO's, (3) electric-quadrupole interactions at both metal-ion sites measured at approximately 800 K (above T_N) on most of the REO's and (4) temperature dependence of the combined interactions at the Fe sites for several REO's, in which the MHF is strong, i.e., $y > 10$, at temperatures well below T_N.

Figure 4 presents laboratory-temperature perturbation functions and the corresponding Fourier transforms for some of the REO's. For the compounds containing the heavier rare earths, Dy and Eu, the perturbation functions and transforms are qualitatively very similar, and they show the features of near-axial EFG symmetry. Whereas for the compounds containing the lighter rare earths, La, Nd, and Eu, the perturbation functions show the features of more asymmetry. The near degeneracy of the frequencies ω_2 and ω_5 is evident. The low-frequency peak in the transform that contains the frequencies ω_1 and ω_4 splits into two distinguishable peaks as the rare-earth atomic number Z increases. These peaks represent transitions between $m=-\frac{3}{2}$ and $-\frac{1}{2}$ and $m=\frac{3}{2}$ and $\frac{1}{2}$, respectively. Thus, the MHI lifts the degeneracy of the $m=\pm\frac{1}{2}$ states that gives rise to the splitting of the low-frequency peak. However, as Fig. 5 shows, y remains relatively constant as Z increases even though ω_1 and ω_4 become more different in value as Z increases. The magnitude of y changes very little with increasing Z, presumably, because η decreases and β and V_{zz} increase somewhat as Z increases.

Figure 5 summarizes the parameters that we obtained by first fitting the perturbation functions for the laboratory-temperature measurements using Eq. (2) to obtain the ω_i's and the other parameters and second minimizing χ^2 given by Eq. (3) to obtain η, y, β, and α. Typical magnitudes of the grid-search parameter intervals were $\Delta\eta=0.02-0.04$, $\Delta y=0.01-0.03$, $\Delta\beta=1°-3°$,

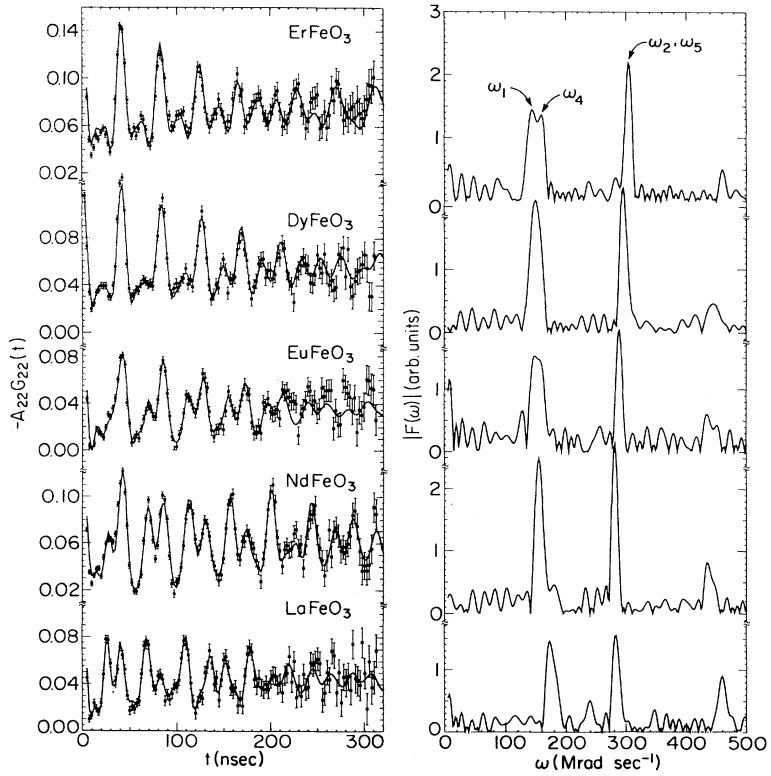

FIG. 4. Perturbation functions and Fourier transforms for several REO's measured at laboratory temperature. The solid lines on the perturbation functions represent fits of Eq. (2) to the data. In these measurements, the primary interactions occurred at the rare-earth sites, where the nuclear-quadrupole interaction was large and the magnetic hyperfine interaction was weak.

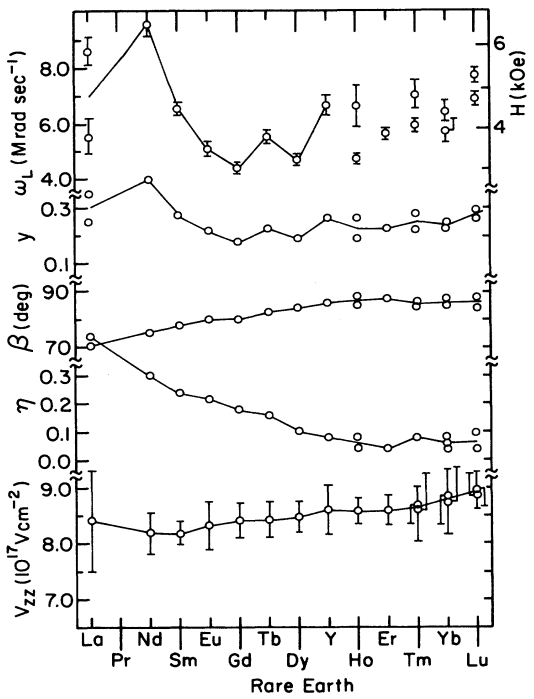

FIG. 5. Derived parameters that represent the laboratory-temperature measurements of rare-earth-site combined interactions. The double data points, which appear for some of the REO's, indicate results of measurements on duplicate samples, and for $PrFeO_3$ we could not resolve the interaction parameters for the Pr site. The errors shown on the V_{zz} values appear to be too large because they include the effects of the large statistical uncertainties in the ω_1 and ω_5 values.

and $\Delta\alpha = 15°$ ($0° \leq \beta \leq 90°$ and $0° \leq \alpha \leq 90°$). To obtain ω_Q from the measured ω_1, ω_2, ω_4, and ω_5 values, we used the derived values of η, y, β, and α to specify the corresponding values of $\Delta E'_{mm}$ in units of $\hbar\omega_Q$. This procedure gave four values of ω_Q. We used the average of these values as the final ω_Q value to which we assigned an uncertainty based on the uncertainties associated with the ω_i values. From these quantities, we calculated the V_{zz} values and the corresponding Larmor-frequency values $\omega_L = y\omega_Q$.

Now, as we discuss in detail below, we assign these parameter values to the rare-earth sites. For most of the heavier REO's (R=Eu,Gd,...,Lu), the probes substituted primarily into these sites. However, in most of these samples, the probes also substituted into the Fe sites to a small extent. At temperatures below T_N, the corresponding Fe-site interactions could not be characterized because the strong MHF's at the Fe sites caused large frequency shifts. However, at temperatures above T_N, the nuclear-quadrupole interactions (NQI's) at both sites could be characterized. We present those results below.

The values of ω_L that Fig. 5 show fluctuate much more in magnitude than the associated errors imply. However, the opposite is the case for the values of V_{zz}. These differences arise for two reasons. First, the values of ω_L are affected strongly by errors that propagate in determining η, y, and β. Second, unlike the ω_L values, the magnitudes of ω_Q and the corresponding V_{zz} values depend very weakly on the parameters η, y, and β. Instead, the accuracy of ω_Q depends strongly on the accuracy with which ω_2 and ω_5 are determined as well as on the average of ω_1 and ω_4. In this particular situation, in which y and η are small and $\beta \approx 90°$, ω_2 and ω_5 can be

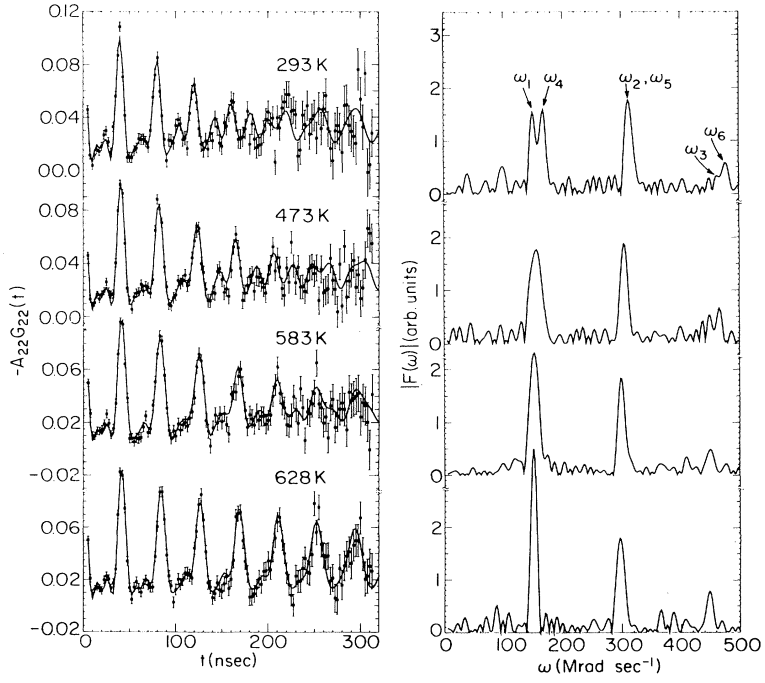

FIG. 6. Perturbation functions and Fourier transforms for a $LuFeO_3$ sample measured at the indicated temperatures. The solid lines on the perturbation functions represent fits of Eq. (2) to the data. In the transforms, the effects of temperature are clearly evident in the widths and amplitudes of the doublets that represent ω_1 and ω_4.

measured to accuracies of several percent, and the average of ω_1 and ω_4 tends to be reliable, even though the errors in the individual values of ω_1 and ω_4 are often large. When the MHI is very weak, as in the case in this situation, the Larmor frequency ω_L cannot be measured accurately; whereas, the strong electric-quadrupole interaction can be accurately characterized by the V_{zz} and η values. In addition, as the rare-earth atomic number Z decreases, the EFG component V_{zz} decreases slowly, and the associated asymmetry η increases. The parameters β and y do not show a strong dependence on Z. The increase in the η values that occurs as Z decreases is particularly unexpected. The lattice parameters for $LaFeO_3$ represent near tetragonality, i.e., $a=5.556$ Å, $b=5.565$ Å, and $c=7.862$ Å; whereas, the lattice parameters for $LuFeO_3$ represent a large orthorhombic distortion, i.e., $a=5.213$ Å, $b=5.547$ Å, and $c=7.565$ Å.[6] Thus, the more symmetric crystals, i.e., those that have lower Z values, show more asymmetric EFG's and vice versa. This result suggests that at the rare-earth sites in the REO's the EFG principal axes may not be aligned with the crystallographic axes.

Figure 6 presents some perturbation functions and the corresponding Fourier transforms for a sample of $LuFeO_3$ measured at a series of temperatures. This figure shows clearly that the splitting of the frequencies ω_1 and ω_4 decreases as temperature increases. Figure 7 summarizes the temperature dependences of the parameters derived from the fits of Eq. (2) to the perturbation functions for samples of $LuFeO_3$ and $HoFeO_3$. Similar plots for $EuFeO_3$, $YFeO_3$, and $YbFeO_3$ show the same qualitative features. These summaries indicate that the combined-interaction parameters ω_1, ω_4, R_{21}, and R_{54} become indeterminate as the temperature approaches T_N. The onset of the indeterminacy occurs at roughly 100 K below T_N. For this reason, details of the MHI, such as critical phenomena, cannot be observed reliably at temperatures near T_N. For most of the measurements, the values of the line-shape parameters δ are small and reasonably constant, and the site-occupancy fractions f are reasonably large and constant. The ratio S_1/S_4 provides a check on the consistency of the fits to the perturbation functions. As ω_1 and ω_4 approach each other in value, we expect the fitting procedure to fail to be able to separate these frequency components. Large errors in the ratio as well as in the corresponding values of ω_1, ω_4, R_{21}, and R_{54} indicate when this situation occurs. We see that the procedure fails for data collected at temperatures that are well below T_N. For the same compounds, Fig. 8 presents the temperature dependences of the quantities V_{zz}, η, β, y, and ω_L that we derived from the primary parameters that Fig. 7 presents. For V_{zz}, η, β, y, the lines in Fig. 8 represents least-squares fits to each corresponding set of

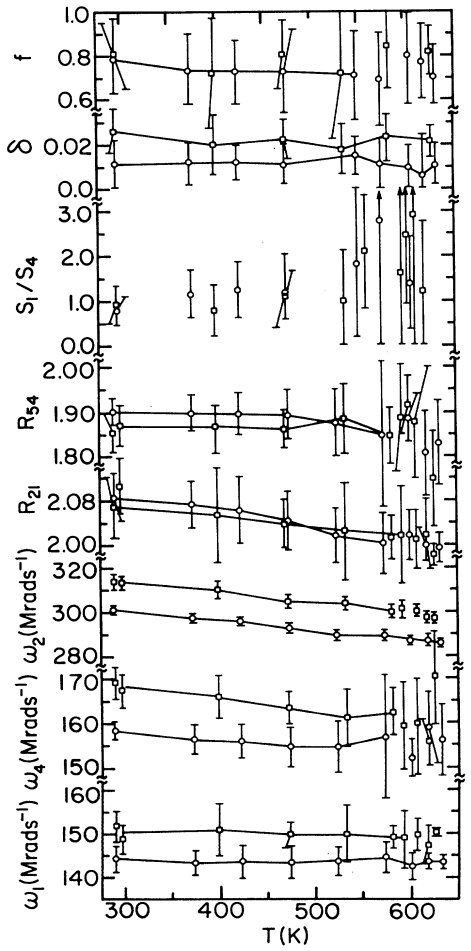

FIG. 7. Temperature dependence of the major interaction frequencies and related parameters for the combined nuclear-quadrupole weak-magnetic-dipole interactions. The circles represent data points for $HoFeO_3$ and the squares represent data points for $LuFeO_3$.

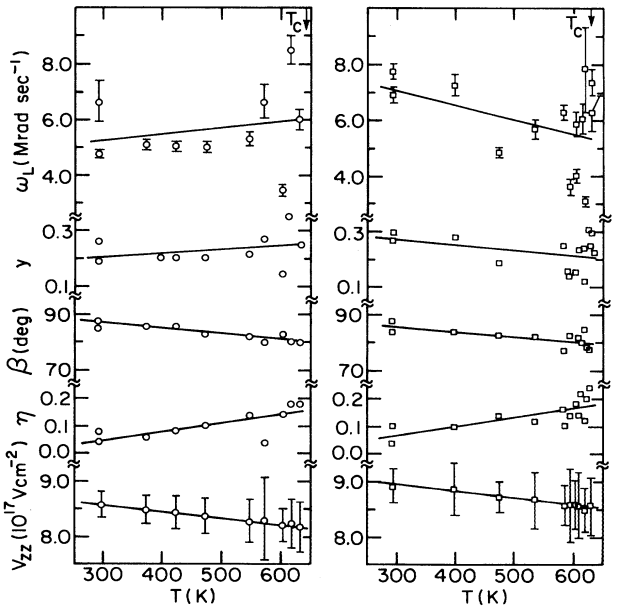

FIG. 8. Temperature dependence of the parameters derived from the major interaction frequencies that Fig. 7 presents. The left figure shows parameters for $HoFeO_3$, and the right figure shows those for $LuFeO_3$. For both compounds, V_{zz}, η, and β show linear temperature dependences, and the corresponding lines represent least-squares fits.

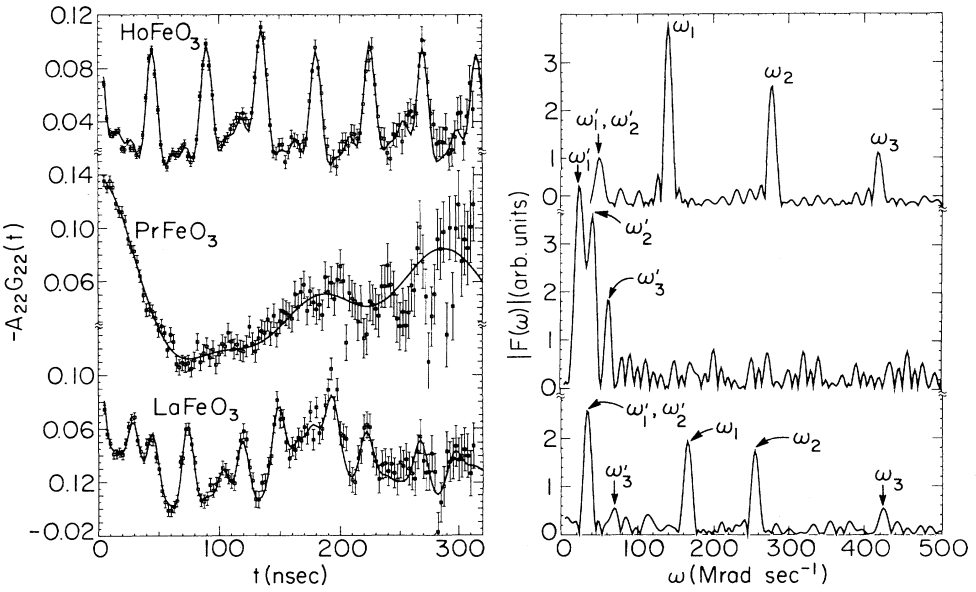

FIG. 9. Perturbation functions and Fourier transforms measured at 800 K. For $HoFeO_3$, the functions and transforms show primarily a high-frequency nuclear-quadrupole interaction, which we assign to the Ho site, although a small low-frequency component is also evident. For $PrFeO_3$, the functions and transforms show primarily a low-frequency interaction, which we assign to the Fe site. For $LaFeO_3$, both low-frequency and high-frequency interactions are evident.

data points. As we mentioned above, the values of ω_L have large uncertainties that error propagation produced. For this reason, we obtained the lines indicated for the ω_L values by multiplying the linear fits to the corresponding values of y and V_{zz} because the lines for y and V_{zz} represent averages.

Figure 9 presents the perturbation functions and the corresponding Fourier transforms for several REO's measured at an arbitrarily chosen temperature 800 K, which is well above T_N. In the case of the $HoFeO_3$ sample, the probe substituted primarily into a site where the EFG was large and nearly axially symmetric, although a low-frequency peak indicates that a small fraction of the probes substituted into a different well-defined site. In the case of the $PrFeO_3$ sample, the probe substituted primarily into a site where the EFG was small and asymmetric. In the case of the $LaFeO_3$ samples, the probe substituted into both well-defined sites in which the ratio of high-frequency to low-frequency site occupancy was approximately 10:7. Figure 10 presents a summary of the parameters derived from the high-temperature (either near or at 800 K) measurements. For the high-frequency interactions, the trends in the values of V_{zz} and η are similar to those measured at laboratory temperature, which Fig. 5 summarizes. The EFG's decrease in magnitude and increase in asymmetry as the rare-earth Z values decrease. For the low-frequency interactions, the EFG's decrease slowly as Z decreases, and they are all very asymmetric. The changes in the η values that do not correlate with the corresponding changes in lattice parameters suggest that the EFG principal axes at these sites may not be aligned with the crystallographic axes. The ratios of the high-frequency-interaction values to the low-frequency-interaction values of V_{zz} are 6.2 ± 0.3 for $LaFeO_3$ and 3.9 ± 0.2 for $LuFeO_3$. Here we see that at neither probe site does the variation in the measured η values correlate with the corresponding changes in lattice parameters.

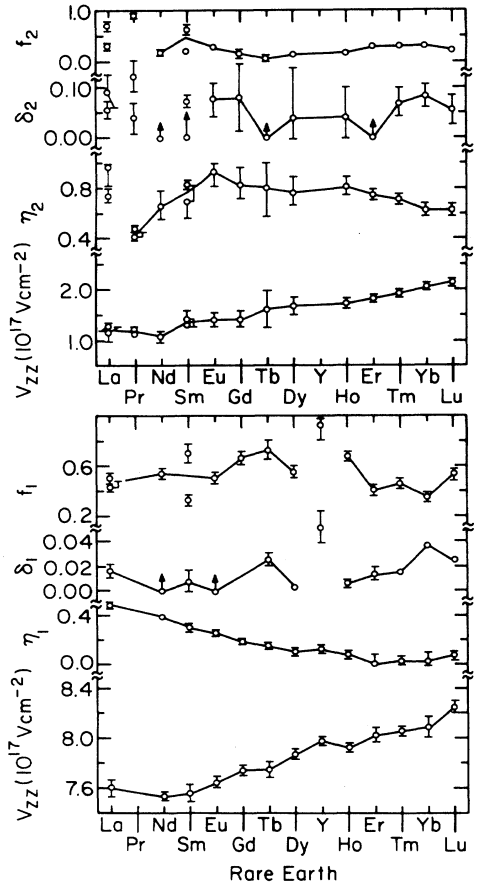

FIG. 10. Summary of the parameters derived from the fits of Eq. (1) to the perturbation functions measured either at or near 800 K. The upper figure presents parameters that represent the low-frequency nuclear-quadrupole interactions, which we assign to the Fe sites. The lower figure presents parameters that represent the high-frequency interaction, which we assign to the rare-earth sites.

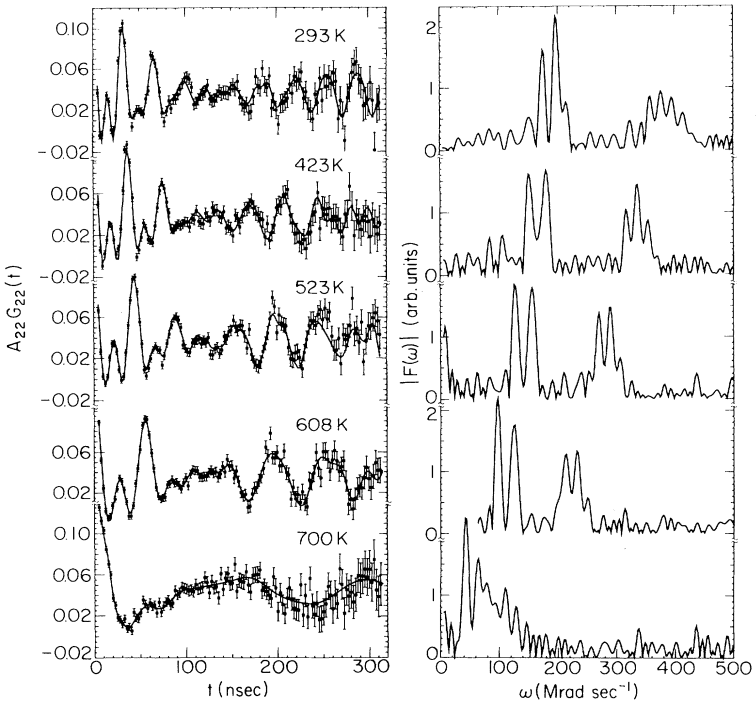

FIG. 11. Perturbation functions and Fourier transforms for $PrFeO_3$ measured at the indicated temperatures. The solid lines on the perturbation functions represent fits of Eq. (2) to the data.

Figure 11 presents some of the perturbation functions and Fourier transforms for $PrFeO_3$ samples measured at a series of temperatures below T_N.[30] We see that the frequency splitting by a strong MHF is an extremely large effect that has a very strong temperature dependence. In particular, the MHI produces two sets of frequencies. At high temperatures, e.g., 700 K, which are close to T_N, one set of frequencies is centered in the transform at approximately 45 Mrad sec^{-1} and the other appears over the range from 60 to 140 Mrad sec^{-1}. At lower temperatures, two sets of frequencies are also evident but the splittings are much larger. Also, the peak at approximately 25 Mrad sec^{-1} that represents the pure quadrupole-interaction frequency ω_1, which Fig. 9 shows, is missing.

IV. DISCUSSION

A. Site substitution of the probe

The probe-site assignment is at first consideration not obvious. We observed two well-defined electric-quadrupole interactions; for the heavier REO's one is characterized by low frequencies and by small site-occupancy fractions and the other is characterized by high frequencies and by large site-occupancy fractions. For the high-frequency site, as Fig. 10 indicates, the EFG asymmetry η increases as the rare-earth atomic number decreases. This result is in contradistinction to the corresponding trend in the lattice parameters, which indicates that $LaFeO_3$ has the most symmetric structure and $LuFeO_3$ has the least. For the low-frequency site, the EFG asymmetries are all large. However, according to the crystal-structure analysis,[5,28] the Fe oxygen octahedra in the REO's are symmetric, and, as the rare-earth ionic size decreases (Z becomes larger), the crystal structures become more distorted as the corner-shared Fe oxygen octahedra tilt more with respect to each other. In addition, the ionic radii for six coordination are 0.785 Å, for Fe^{3+} high-spin ions, 1.185 Å for La^{3+} ions, 1.001 Å for Lu^{3+} ions, and 0.94 Å for In^{3+} ions. This information suggests that the Fe-site size and symmetry change very little and that the rare-earth site size changes considerably as the rare-earth composition changes. Also, on the basis of ionic-radii considerations, we would expect the ^{111}In probe to be more likely to substitute into the rare-earth sites in the heavier REO's. For the lower-atomic-number REO's, the site substitution depends on the thermal processing conditions. Unfortunately, much of this crystal-chemistry information is either circumstantial, i.e., the ionic-radii considerations prove little, or mutually inconsistent, i.e., the EFG asymmetries do not suggest a consistent set of site assignments.

To make the probe-site assignments, we consider two experimental results. First, using ME spectroscopy, Eibschütz, Shtrickman, and Treves[5] measured the Fe-site quadrupole-coupling constant, which they gave as $\varepsilon = -3eV_{zz}/4I(2I-1)$. Although the electric-quadrupole interaction was a very weak effect in their experiments that they could not measure accurately, their results are sufficiently good so that we can estimate the EFG that the ^{111}Cd probe nucleus would measure at an Fe site in one of the REO's. They reported $/\varepsilon/$ values that ranged up to approximately 0.03 mm sec^{-1}, which corresponds to $V_{zz} \approx 2.8 \times 10^{16} V$ cm^{-2}, using $Q = 0.21$ b for the ^{57}Fe quadrupole moment. We multiply this value of V_{zz} by the ratio of Sternheimer antishielding factors[29] (30.3/10.14) to obtain $V'_{zz} \approx 8.2 \times 10^{16}$ V cm^{-2}. For the

high-frequency interaction, the smallest values of V_{zz} that we observed are approximately 8×10^{17} V cm^{-2}. This order-of-magnitude difference is well in excess of the difference that the combined uncertainties in the reported value of the ^{57}Fe quadrupole moment and in the antishielding factor ratio could produce, which we estimate to be a factor of 4 in the adjusted value of V'_{zz}. For the low-frequency interaction, the V_{zz} values that we observed are approximately $1-2\times10^{17}$ V cm^{-2}, and these values are reasonably close to this estimate of V'_{zz}, which represents our expected value of V_{zz} at the Fe site.

Second, we consider the magnitude of the MHF at the sites where we observed low-frequency electric-quadrupole interactions. Based on the theoretical analysis of hyperfine fields in REO's,[15] and on the experimental measurements of STHF's in similar perovskites,[20,21] we expect that a STHF would have a magnitude on the order of 100 kOe. Specifically, in $PrFeO_3$ and $NdFeO_3$, at temperatures of several hundred K, we did observe strong MHI's at sites where the low-frequency electric-quadrupole interaction occurs, and the magnitudes of these MHI's are consistent with this expectation.

The directional bonding through corner-shared octahedra via Fe—O—Fe bonds provides a direct pathway for STHF, when a ^{111}Cd atom substitutes for an Fe atom. Thus, using this information, we assign the low-frequency electric-quadrupole and high-frequency magnetic-dipole interactions to the Fe sites in the REO's.

In contradistinction to the nearly linear Fe—O—Fe bonds, the Fe—O—*R* bonds range in angle from $\approx80°$ to $\approx120°$, i.e., the bonds are nearly perpendicular. Additionally, the *R*—O bonds, which typically are 2.3–2.8 Å, are much longer than the Fe—O bonds, which typically are ≈2 Å.[30] Thus, the directional-bonding pathway for spin-density transfer from the Fe ions through the O ligands to ^{111}Cd ions at the rare-earth sites is not geometrically favorable for producing large STHF's at the ^{111}Cd nuclei. This situation, however, does not rule out the possibility that weak STHF's could occur at the rare-earth sites. As Fig. 5 shows, at the site where we observed the high-frequency electric-quadrupole interaction, typical values of the corresponding Larmor frequency are approximately 6 Mrad sec^{-1}, which corresponds to a MHF of about 4 kOe. Moreover, from symmetry considerations, dipole fields at the rare-earth sites that *pure* antiferromagnetic ordering of the Fe-site magnetic moments would produce should vanish. The small degree of canting that produces small dipole fields and makes the REO's weakly ferromagnetic is insufficient by at least an order of magnitude to account for the observed MHF's. Thus, considering the MHF and EFG magnitudes, we assign the combined low-frequency magnetic-dipole and high-frequency electric-quadrupole interactions to the rare-earth sites.

B. Weak MHF at the rare-earth sites

Figure 4 shows a representative series of laboratory-temperature perturbation functions and the associated Fourier transforms. The transforms clearly indicate that, as the rare-earth atomic number *Z* increases, the rare-earth-site EFG's become more symmetric, i.e., $\eta\rightarrow0$, and the splitting of the $\omega_1-\omega_4$ peak becomes larger. Unfortunately, the derived Larmor frequencies ω_L that Fig. 5 shows do not show a trend with changes in *Z* that is discernible above the scatter in the data points. For $LuFeO_3$, Fig. 6 shows the perturbation functions and Fourier transforms measured at several successively higher temperatures, and Fig. 8 summarizes the derived parameters. Because significant uncertainties are associated with the ω_L values, we have insufficient information with which to characterize the temperature dependence of the MHF associated with these values. To a good approximation, ω_L has a constant temperature dependence, except perhaps at temperatures near T_N where we are unable to measure it. In lieu of using the ω_L temperature dependence to infer the origins of the weak MHF's, we speculate that the observed weak MHF could be a STHF that spin transferred through nearly 90° Fe—O—Cd bonds produces. Generally in ABO_3 perovskites, in which *B* represents a transition metal, the effects of superexchange and the magnitudes of MHF's tend to be enhanced as the *B*-ion–ligand–*B*-ion (or *B*-ion–ligand–Cd ion) bonds increase toward 180° because the overlap between the transition-metal d_{z^2} and O p_z orbitals increases.[15,21] Alternatively, when the directional-bonding pathway between two metal ions and a ligand involves bond angles that are closer to 90° than to 180°, the MHF's as well as the effects of superexchange tend to be weak. This situation arises because the overlap between the O *p* orbitals and the Cd 4*s* and 5*s* orbitals is small. As far as we know, no other measurements of the *A*-site STHF's in ABO_3 perovskites have been reported. Since this report may be the first of an *A*-site STHF, the measured rare-earth-site MHF's in the REO's are now an experimental benchmark for measurements on other perovskites and for more detailed calculations.

Furthermore, for the heavier REO's, the angles β between the direction of the MHF and the *z* axis of the EFG are nearly 90°, and these angles decrease slowly as the rare-earth atomic number *Z* decreases. However, the direction of the EFG *z* axis is not apparent. The distortion of the rare-earth polyhedra suggests that the rare-earth-site EFG's should be very asymmetric. Moreover, as *Z* increases, the lattice parameters *a* and *b* differ more and more in value, i.e., the orthorhombic distortion increases as *Z* increases. As the crystal distorts more, we would expect the EFG asymmetry η to increase. But, for the heavier REO's, the η values show that the EFG's are nearly axially symmetric. This apparent inconsistency strongly suggests that the EFG axes are not aligned with the crystallographic axes. Thus, the measured EFG parameters V_{zz} and η and the angle β provide constraints for any theoretical model that includes structural and magnetic effects.

C. Strong MHI at the Fe sites

In the lighter REO's, $LaFeO_3$, $PrFeO_3$, $NdFeO_3$, and $SmFeO_3$, and perhaps others, we can substitute the ^{111}In probe primarily into the Fe sites by adjusting the sinter-

ing temperature, although we have not systematized this effect yet. In polycrystalline samples of magnetic materials that have cubic crystal symmetry and vanishing probe-site EFG's, pure MHI's can be observed. When the probe occupies a single well-defined site, the associated perturbation functions contain primarily two frequency components ω_L and $2\omega_L$. The ω_L frequency component represents five degenerate $m-m'=\pm 1$ transitions, and the $2\omega_L$ component represents four degenerate $m-m'=\pm 2$ transitions. When a relatively weak electric-quadrupole interaction arises because the crystal has lower-than-cubic symmetry at the probe site, this interaction lifts the degeneracies of the ω_L and $2\omega_L$ components. As a result, at the Fe sites, we expect to observe two sets of frequency components, a lower set that contains five components, which has an average value that is near ω_L, and a higher set that contains four components, which has an average value that is near $2\omega_L$. Depending on the strength, symmetry, and orientation of the EFG tensor with respect to the MHF direction, some of these frequency components may be nearly degenerate, and, consequently, they may be experimentally unresolvable.[31] Unfortunately, because we do not know the aforementioned EFG characteristics *a priori*, we do not know which specific components may be unresolvable. We found that up to four of the five low-frequency components and up to four of the four high-frequency components could be determined by fitting Eq. (2) to the lower-temperature perturbation functions. The higher-temperature perturbation functions generally yielded fewer components. Thus, the absence of one or more frequency components complicates and limits the complete analysis. In addition to this problem, the presence of other frequency components in the perturbation functions further complicates the analysis. These other components may arise as a result of interactions other than the primary combined interaction, e.g., rare-earth-site interactions.

To systematize the frequency components obtained from the fits, we use the power-law dependence of the frequencies on reduced temperature, which Fig. 12 shows for $PrFeO_3$. For the larger reduced temperatures, the low frequencies and high frequencies each form four loci. For the smaller reduced temperatures, ambiguity arises in assigning the corresponding frequencies to the loci that we established using the lower-temperature data. For this reason, to apply the power law, we selected frequency values for which the reduced temperature is in the range $0.1 \le t_r \le 0.4$, $t_r = 1-(T/T_N)$, except for the lowest-frequency locus that we could extend down to $t_r \approx 0.02$. We subsequently fitted these loci to straight lines on logarithmic coordinates: $\omega_i(t_r)=\omega_i(0)t_r^{\beta}$, which gave an average value $\beta=0.35\pm 0.02$. (The exponent β is not to be confused with the angle β.) This β value is in good agreement with the MHF critical exponent measured by ME spectroscopy on $PrFeO_3$, $\beta=0.345\pm 0.005$.[5] (Because $t_r > 0.1$, our values may not reflect actual critical behavior.)

To further analyze this frequency information for $PrFeO_3$, we selected frequency sets at temperatures for which all four high-frequency components are resolved.

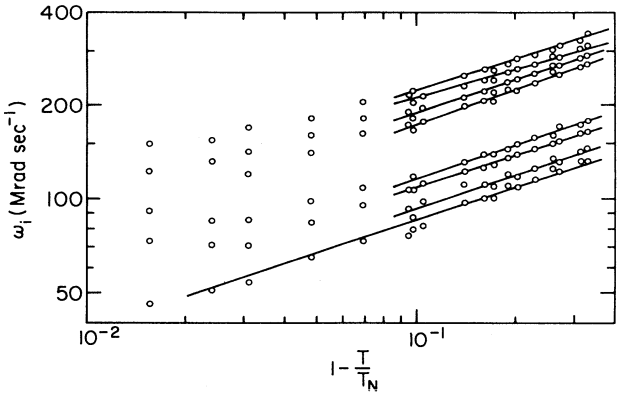

FIG. 12. Power-law dependence of the interaction frequencies for $PrFeO_3$.

We applied the parameter search method described above. In this search, we fixed $\eta=0.44\pm 0.03$ and $\omega_Q=3.53\pm 0.03$ Mrad sec^{-1}, which are the average values measured at 800 K. Over the range of temperature from 470 to 645 K, we obtained an average value of the angle $\beta=40°\pm 2°$ for $\alpha=0°$. For other values of $\alpha=30°$, 60°, and 90°, the searches produced values of χ^2 that are significantly higher, and they produced corresponding values of β that are systematically lower, 38°, 35°, and 34°, respectively. Figure 13 shows the dependence of the measured frequency components ω_i on the parameter y. We see qualitatively that the theoretical frequencies for the indicated fixed parameters provide a good representation of the data. This agreement supports the tacit assumption that the 800-K values of ω_Q and η have a weak temperature dependence.

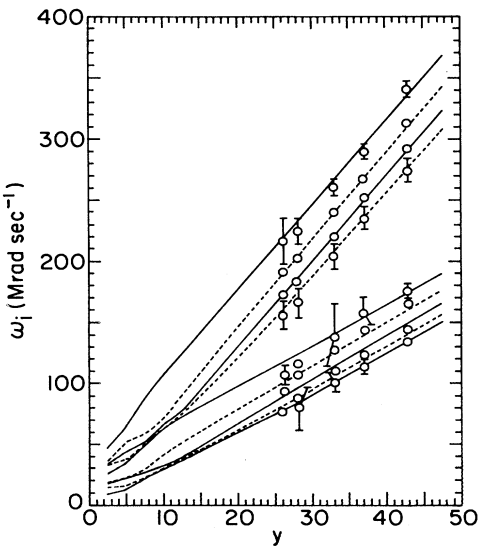

FIG. 13. Dependence of the interaction frequencies ω_i on the parameter y, in which $\eta=0.44$, $\beta=40°$, $\alpha=0°$, and $\omega_Q=3.53$ Mrad sec^{-1}. The lines represent frequencies that were obtained from the eigenvalues of the Hamilton matrix, which were initially calculated in units of $\hbar\omega_Q$. The y axis was calibrated using this value of ω_Q. The data points represent *selected sets* of the measured interaction frequencies that appear in Fig. 12.

In addition to analyzing the strong Fe-site MHI's in $PrFeO_3$, we analyzed similar measurements on $NdFeO_3$. For $NdFeO_3$, we obtained fewer measurements, and Fig. 14 presents the power-law representation. The loci that we were able to fit to straight lines gave an average value of the exponent $\beta=0.41\pm0.02$. Subsequent searching for the angle β, yielded $\beta=40°\pm2°$ for $\alpha=0°$, in which the 800-K EFG values were fixed at $\omega_Q=3.28\pm0.11$ Mrad sec^{-1} and $\eta=0.59\pm0.07$. Again, the $\alpha=0°$ values gave the lowest χ^2 values. Thus, the angle β between the MHF direction and the EFG z axis are essentially the same for $PrFeO_3$ and $NdFeO_3$, and the value of $\beta=40°$ and $\alpha=0°$ best represent the MHI.

To compare the MHF information that we obtained from PAC measurements to other experimental and theoretical information, we approximated ω_L by averaging the four high-frequency loci in Fig. 12 at a specific temperature such as 0 K. We obtained $\langle\omega_L\rangle=220\pm10$ Mrad sec^{-1}, and using $g=-0.306$, we obtained the MHF $|H|=150\pm7$ kOe. The MHF measured by ME spectroscopy is 559 kOe at 0 K. Boekema, Van der Woude, and Sawatzky[15] developed a quantum-chemistry theory of the MHI's in the REO's, in which they express the MHF as

$$H=H_{\text{free}}+H_{\text{cov}}+H_{\text{STHF}} . \tag{5}$$

H_{free} represents the free-ion hyperfine-field component, H_{cov} represents the covalent component, and H_{STHF} represents the supertransferred component. To test the theory, they only had the ME results available. They extrapolated the 0-K values of the ME measured MHF's for the REO's to obtain a MHF value that corresponds to the Fe—O—Fe bond angle of 180°. Then they set the extrapolated value (to which they assigned a minus sign) equal to the total MHF given by Eq. (5), i.e., $H=-576$ kOe. They used $H_{\text{free}}=-630$ kOe. Subsequently, from their theory, they obtained $H_{\text{STHF}}=-104$ kOe and $H_{\text{cov}}=158$ kOe. For the case of $PrFeO_3$ in which the Fe—O—Fe bond angle $\theta=153°$, we assume that H_{cov} and H_{free} do not depend on θ, and we obtain a value of $H_{\text{STHF}}=-86$ kOe, which is less in magnitude than their corresponding value for $\theta=180°$, i.e., -104 kOe. Based on the approach used in the earlier PAC studies,[20,21] we identify the MHF measured by ^{111}Cd PAC as "the STHF" $(|H_{\text{STHF}}|)_{\text{PAC}}=150\pm7$ kOe. We see that it agrees within approximately a factor of 2 with the magnitude of the adjusted value obtained from the quantum-chemistry theory, namely, 86 kOe.

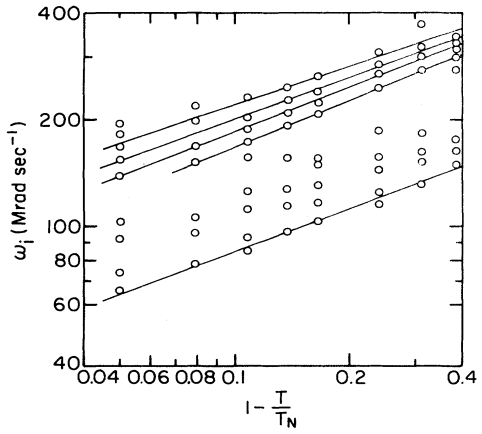

FIG. 14. Power-law dependence of the interaction frequencies for $NdFeO_3$.

Now, we treat the PAC-measured quantity $(|H_{\text{STHF}}|)_{\text{PAC}}$ as if it were the same as the STHF component that is present at the native Fe nuclei. However, the $^{111}Cd^{2+}$ probe ion differs from the Fe^{3+} ion in electronic structure, which introduces an uncertainty into this comparison. The primary contribution to the STHF arises from spin density transferred directly into Cd^{2+} 4s and 5s orbitals, and the spin density transferred into the 4s orbitals makes the most significant contribution to the STHF.[20,21] Differences between the p and d orbitals of the Fe^{3+} and Cd^{2+} ions should not strongly affect the STHF, although these differences may affect the metal-oxygen bonding. Thus, we expect differences between the shapes of the Fe^{3+} 4s and the Cd^{2+} 4s orbitals to be responsible for any major differences between the native-ion STHF and the PAC-measured quantity. This information, which we base on the theoretical and experimental results given in Refs. 20 and 21 that include the values of O p-orbital and transition-metal and Cd s-orbital overlap integrals, suggests that the native-ion STHF and the PAC-measured STHF do not differ greatly. A better theoretical analysis is needed to completely resolve this question.

Despite this particular limitation, the PAC measurement of the Fe-site MHF does provide different information that complements the values of H measured by ME spectroscopy. It gives (within the aforementioned limitation) H_{STHF} in the absence of H_{free} and H_{cov}. This quantity provides an independent reference point to which theoretical calculations can be compared. Moreover, the estimates of the angle β that the PAC measurements also provide establish additional benchmarks to which theory can be compared. In this context, a more-detailed theory is needed. A theory that could be used to calculate both EFG's and MHF's could be tested directly using the information that the PAC experiment provides.

In addition, although we used the power-law dependence of the interaction frequencies ω_K as a means to help determine the MHF parameters, we did, in fact, also determine the Fe-site STHF temperature dependence, and it is very similar to the temperature dependence of the total MHF measured by ME spectroscopy. We did not, however, attempt to measure critical effects at temperatures very near T_N. But the results strongly suggest that critical effects associated with the STHF at the Fe sites in the REO's could be measured. Although the individual frequencies ω_k could not be resolved at small t_r, the average values that closely approximate either ω_L or $2\omega_L$ may be measurable, at least down to some range of small t_r values. Since, as $T\rightarrow T_N$, $y\rightarrow0$, the dependence on y of the frequencies ω_k and their corresponding amplitudes S_k changes very rapidly. For this reason, searching for critical effects may be a very interesting as well as a rather unpredictable experiment.

V. CONCLUSIONS

Combined magnetic-dipole and electric-quadrupole interactions can be measured at both the rare-earth and Fe sites in the REO's using the $^{111}In \rightarrow ^{111}Cd$ probe. This probe substitutes primarily into the rare-earth sites in the heavier REO's, and, depending on the thermal processing conditions, it substitutes into either or both metal-ion sites in the lighter REO's.

The combined interactions at the rare-earth sites involve high-frequency electric-quadrupole interactions and relatively weak magnetic-dipole interactions. Spin density transferred via near-90° Fe—O—^{111}Cd bonds may produce these weak magnetic-dipole interactions. The directions of these weak STHF's are nearly perpendicular to the corresponding rare-earth-site EFG principal z axes.

The combined interactions at the Fe sites involve low-frequency electric-quadrupole interactions and relatively strong magnetic-dipole interactions. The magnetic dipole interactions could be attributed to the presence of STHF's at the probe sites that arise from the transfer of spin density via large-angle Fe—O—^{111}Cd bonds. The corresponding STHF temperature dependences (over the experimentally accessed temperature range) are very similar to the temperature dependences of the total MHF. The strengths of these STHF's agree to within approximately a factor of 2 with the predictions of a quantum-chemistry theory of MHI's in the REO's. Moreover, this experiment demonstrates that PAC can be used to measure STHF's in very asymmetric, magnetically ordered ternary metal-oxide crystals. Thus, these measurements along with future PAC measurements on other crystals can provide new information, namely, the direction and magnitude of the STHF's in the absence of the d-electron-produced MHF, which can then be used to develop more detailed and accurate theories.

ACKNOWLEDGMENTS

We thank Professor David A. Shirley for reviewing this research and for providing many important suggestions. We thank Professor Robert L. Rasera of the University of Maryland Baltimore County for strongly encouraging us to investigate combined hyperfine interactions. We thank Dr. Susan L. Hoyle and Professor Deane K. Smith of the Materials Research Laboratory for helping us to understand the crystal structures. We gratefully acknowledge support for this project from the Office of Naval Research (Grant No. N00014-90-J-4112).

[1]A. A. Mukhin, A. Yu. Pronin, A. S. Prokhorov, G. V. Kozlov, V. Zeleny, and J. Petzelt, Phys. Lett. A **153**, 499 (1991).
[2]T. Peterlin-Neumaier and E. Steichele, J. Magn. Magn. Mater. **59**, 351 (1986).
[3]S. Venugopalan, M. Dutta, A. K. Ramdas, and J. P. Remeika, Phys. Rev. B **27**, 3115 (1983).
[4]R. L. White, J. Appl. Phys. **40**, 1061 (1969).
[5]M. Eibschütz, S. Shtrikman, and D. Treves, Phys. Rev. **156**, 562 (1967).
[6]D. Treves, J. Appl. Phys. **36**, 1033 (1965).
[7]W. C. Koehler, E. P. Wollan, and M. K. Wilkinson, Phys. Rev. **118**, 58 (1960).
[8]S. Venugopalan and M. M. Bercker, J. Chem. Phys. **93**, 3833 (1990).
[9]R. M. White, R. J. Nemanich, and C. Herring, Phys. Rev. B **25**, 1822 (1982).
[10]A. K. Zvezdin and V. M. Matveev, Zh. Eksp. Teor. Fiz. **77**, 1076 (1979) [Sov. Phys. JETP **50**, 543 (1979)].
[11]K. P. Belov, A. K. Zvezdin, A. M. Kadomtseva, I. B. Krynetskii, and V. M. Martveev, Fiz. Tverd. Tela (Leningrad) **19**, 259 (1977) [Sov. Phys. Solid State **19**, 149 (1977)].
[12]J. C. Walling and R. L. White, Phys. Rev. B **10**, 4748 (1974).
[13]R. Bidaux, J. E. Bouree, and J. Hammann, J. Phys. Chem. Solids **35**, 1645 (1974).
[14]R. Bidaux, J. E. Bouree, and J. Hammann, J. Phys. Chem. Solids **36**, 655 (1975).
[15]C. Boekema, F. Van der Woude, and G. A. Sawatzky, Int. J. Magn. **3**, 341 (1972).
[16]E. Matthias and W. Schneider, Phys. Rev. **125**, 261 (1962).
[17]K. Alder and R. M. Steffen, Phys. Rev. **129**, 1199 (1963).
[18]E. Matthias, B. Olson, and W. Schneider, Ark. Fys. **24**, 245 (1963).
[19]E. Matthias, W. Schneider, and R. M. Steffen, Ark. Fys. **24**, 97 (1962).
[20]H. H. Rinneberg and D. A. Shirley, Phys. Rev. B **13**, 2138 (1976).
[21]H. H. Rinneberg and D. A. Shirley, Phys. Rev. Lett. **30**, 1147 (1973).
[22]D. A. Shirley, S. S. Rosenblum, and E. Matthias, Phys. Rev. **170**, 363 (1968).
[23]D. A. Shirley and G. A. Westenbarger, Phys. Rev. **138**, A170 (1965).
[24]For a review of this work, see C. Hohenemser, N. Rosov, and A. Kleinhammes, Hyperfine Interact. **49**, 267 (1989), and references therein.
[25]J. Saylor, L. Takacs, C. Hohenemser, J. I. Budnick, and B. Chamberland, Phys. Rev. B **40**, 6854 (1989).
[26]G. L. Catchen, L. H. Menke, Jr., K. Jamil, M. Blaszkiewicz, and B. E. Scheetz, Phys. Rev. B **39**, 3826 (1989).
[27]G. L. Catchen, J. Mater. Educ. **12**, 253 (1991).
[28]P. Coppens and M. Eibschütz, Acta Crystallogr. **19**, 524 (1965).
[29]F. D. Feiock and W. R. Johnson, Phys. Rev. **187**, 39 (1969).
[30]M. Marezio, J. P. Remeika, and P. D. Dernier, Acta Crystallogr. B **26**, 2008 (1970).
[31]For a discussion of the sensitivity of PAC measurements to combined interactions in polycrystalline sources see G. L. Catchen (unpublished).